







## Article

# Settlement Analysis of Concrete-Walled Buildings Using Soil–Structure Interactions and Finite Element Modeling

Jonny D. Patrício <sup>1</sup>, Alexandre D. Gusmão <sup>2</sup>, Sílvio R. M. Ferreira <sup>3</sup>, Fernando A. N. Silva <sup>4</sup>,  
Hassan Jafarian Kafshgarkolaei <sup>5</sup>, António C. Azevedo <sup>6</sup> and João M. P. Q. Delgado <sup>5,\*</sup>

- <sup>1</sup> Civil Engineering Department, Federal University of Campina Grande—UFCG, Aprigio Veloso St. Universitário, Campina Grande 58429-900, Brazil; jonny\_dantas@hotmail.com
- <sup>2</sup> Civil Engineering Department, University of Pernambuco—UPE, Benfica St. Madalena, Recife 50720-001, Brazil; gusmao.alex@poli.br
- <sup>3</sup> Centro de Tecnologia de Geociências—CTG, Federal University of Pernambuco—UFPE, Acadêmico Hélio Ramos St., Cidade Universitária, Recife 50740-530, PE, Brazil; silvio.mferreira@ufpe.br
- <sup>4</sup> Civil Engineering Department, Pernambuco Catholic University, Recife 50050-900, Brazil; fernando.nogueira@unicap.br
- <sup>5</sup> CONSTRUCT-LFC, Department of Civil Engineering, Faculty of Engineering, University of Porto, 4200-465 Porto, Portugal; h.jafarian@fe.up.pt
- <sup>6</sup> Federal Institute of Education, Science and Technology of Pernambuco (IFPE), Recife 50670-430, Brazil; antonio.azevedo@caruaru.ifpe.edu.br
- \* Correspondence: jdelgado@fe.up.pt; Tel.: +351-225081404

**Abstract:** This study examines the performance of mat foundations in 13 blocks of eight-story concrete-walled residential buildings. Topographic monitoring bolts were used to monitor the slab's construction, which was 0.35 m thick and comprised an area of 225 m<sup>2</sup>. Using the collected data, a retro-analysis of the modulus of elasticity was conducted to obtain the geotechnical parameters for forecasting the settlement using the elasticity theory. A nonlinear approach for construction modeling and soil–structure interactions showed that the earthworks at the start of construction had a significant role in settling. Blocks in landfills settled faster than those in land-cut zones. The partial execution of building levels was found to be critical in terms of angular distortions and stresses in the concrete slab. The partial lifting of the foundation plate was confirmed in blocks with partial building floor execution, demonstrating the importance of assessing the foundation's behavior at this stage. The modulus of elasticity dropped as construction progressed, with landfill parts being particularly vulnerable. Creep settlements contributed significantly, accounting for about 20% of the total settlements in some blocks. The numerical staged construction model accurately replicated the behaviors observed in the monitoring data, confirming the hypothesis of the partial raising of the foundation during the building process, which resulted in higher angular distortions. Based on the results obtained, the authors strongly recommend that the simultaneous consideration of soil–structure interactions and construction effects be commonly used in foundation designs.

**Keywords:** mat foundations; elastic modulus; soil–structure interaction; raft foundation; settlement measurement



**Citation:** Patrício, J.D.; Gusmão, A.D.; Ferreira, S.R.M.; Silva, F.A.N.; Kafshgarkolaei, H.J.; Azevedo, A.C.; Delgado, J.M.P.Q. Settlement Analysis of Concrete-Walled Buildings Using Soil–Structure Interactions and Finite Element Modeling. *Buildings* **2024**, *14*, 746. <https://doi.org/10.3390/buildings14030746>

Academic Editor: Eugeniusz Koda

Received: 24 January 2024

Revised: 5 March 2024

Accepted: 6 March 2024

Published: 10 March 2024



**Copyright:** © 2024 by the authors. Licensee MDPI, Basel, Switzerland. This article is an open access article distributed under the terms and conditions of the Creative Commons Attribution (CC BY) license (<https://creativecommons.org/licenses/by/4.0/>).

## 1. Introduction

Building systems that combine efficiency and competitiveness have gained significant attention from researchers throughout the world as a result of the fast development of construction technologies in recent years. Among these advances, concrete wall systems and structural blocks have grown in popularity. However, substantial studies on the important subject of soil–structure interactions (SSIs) in these systems are still lacking. Prevalent studies in the literature have ignored SSI issues, particularly for buildings with concrete walls rather than reinforced concrete frame systems. This disparity highlights the need to study the behavior and interactions of this particular building system.

Because of the enhanced construction speed of concrete wall systems, as well as their modular structure and associated improvement in overall structural stiffness, an in-depth analysis is required. This work seeks to address this gap by extensively analyzing the parameters impacting soil–structure interactions and employing numerical modelling. The major focus was on the building of concrete-walled residential structures over reinforced concrete mat foundations. A detailed examination of foundation settlements was a critical component of this assessment, as it allowed for the computation of response coefficients, which were required for the numerical modeling procedure. The study thoroughly explored the intricate behavior of the interaction between the soil and the structure in this building technique using a non-linear finite element analysis.

Furthermore, the present work highlights two key aspects related to the investigation of settlements in mat foundations. To begin, it encourages the use of field-monitored settlement data to precisely establish the elastic modulus, a critical settlement analysis parameter. Second, the research proposes using a factor reduction modulus (FRM) based on the stress levels particular to the mat foundation. These proposed techniques can be used with the aim of increasing the accuracy and utility of settlement evaluations by providing a more sophisticated understanding of the behavior and variables influencing settlement behavior in mat foundation systems.

### *1.1. Brief Literature Review*

The stability and performance of concrete-walled buildings heavily rely on the interaction between the structure and its underlying foundation. Monitoring the mat foundation settlement and employing a soil–structure interaction (SSI) analysis with an elastic modulus back-analysis provides crucial insights into this complex interplay. The most significant research papers in this domain are presented.

Zhang et al. [1] investigated the impact of SSIs on the seismic performance of concrete-walled buildings. The authors developed detailed FE models incorporating soil–structure interactions and analyzed the building’s seismic response under various earthquake scenarios. Their findings highlight the importance of considering SSI effects for earthquake-resistant designs. Bennett et al. [2] designed a real-time monitoring system for mat foundation settlement using wireless sensors. The system continuously transmitted data to a central server, enabling the real-time assessment of settlement behavior and the early detection of potential structural distress. This approach offers invaluable advantages for proactive maintenance and ensuring building safety. Zhu et al. [3] presented a comprehensive investigation of the SSI effects on mat foundation settlement. The authors conducted both physical model tests and FE simulations to analyze the influence of various factors such as the soil stiffness, wall slenderness, and loading conditions. Their findings provide valuable design guidelines for minimizing settlement and ensuring structural integrity. Asli et al. [4] carried out research focused on the retro analysis of the modulus of elasticity of the soil based on measured foundation settlements. The authors used an evolutionary optimization algorithm to iteratively refine the FE model until its predicted settlements matched the measured values. This approach improves the accuracy of the SSI analysis and provides valuable insights into soil behavior. Farias [5] focused on the structural analysis of concrete-walled buildings built on raft foundations while considering soil–structure interactions and progressive vertical loading. The author used the finite element method in DIANA v. 9.4.4 software for numerical simulations and measured the settlement points during construction to evaluate the soil parameters. This approach allows for a comprehensive understanding of the interaction between the structure and the underlying soil. Arteaga et al. [6] employed a combination of settlement points and inclinometers to monitor the foundation behavior of a 10-story concrete-walled building, successfully capturing differential settlements and tilt. Zhussupbekov [7] discussed the technology for supporting excavation structures as a shoring system for concrete-walled constructions on mat foundations. The author mentioned the use of the PLAXIS 2D v. 22.00.00.1733 software to assess deformations and settlements in the soil. This software

provides a valuable tool for analyzing the behavior of the soil–structure system during construction. Bapir et al. [8] proposed an integrated approach involving the combination of in situ settlement sensors with a 3D finite element (FE) SSI analysis. The authors presented a case study of a high-rise concrete-walled building, demonstrating the effectiveness of their method in capturing settlement patterns and evaluating soil–structure interaction effects. Santos et al. [9] focused on the soil–structure interactions (SSIs) in reinforced concrete structures and shallow spread footings. The authors mentioned the use of the elastic theory for estimating the settlement in shallow spread footings and the incorporation of SSI into the structural model for concrete-walled buildings. The influence of the soil stiffness and the relative soil–structure stiffness on the SSI results was also discussed. Further research could explore the impact of different soil and structural parameters on SSI behavior to enhance the accuracy of settlement predictions.

Numerous researchers have conducted parametric studies to investigate the interaction between the soil and surface structures [10–12]. Also, recent studies have compared numerical analysis results with field measurements obtained from constructed projects to analyze the SSIs [13,14]. Because of its industrialized character, the building method employing concrete walls, according to Ng et al. [15], offers advantages such as a quick execution, a reduced amount of manual work required, less expensive overall costs, reduced waste generation, and efficient large-scale manufacturing.

A mat foundation is a shallow foundation that is typically used for structures on soft/weak ground and/or to transmit significant weights to the ground below. It consists of a rigid slab that functions as a single foundation element for the whole structure’s plan area [16].

Mat foundations, like any other type of shallow foundation, should not be allowed to settle excessively. Elastic theory solutions are frequently utilized to examine mat foundation settling. Many strategies for calculating the settling of shallow foundations using the elastic modulus have been described [17–23]. Most of the current approaches for calculating the elastic modulus rely on empirical data acquired from plate load testing [24–26] or penetration testing [27–30].

According to Sharma et al. [31], the elastic modulus of soil is an important characteristic in geotechnical projects, transportation engineering, engineering geology, and geotechnics. Load–settlement relationships are nonlinear [32,33]. This suggests that considering a constant elastic modulus independent of the stress level may underestimate the settlement, as demonstrated by the typical load–settlement curves obtained from a plate load test that showed a smaller elastic modulus as the transmitted stress increased (see Figure 1).

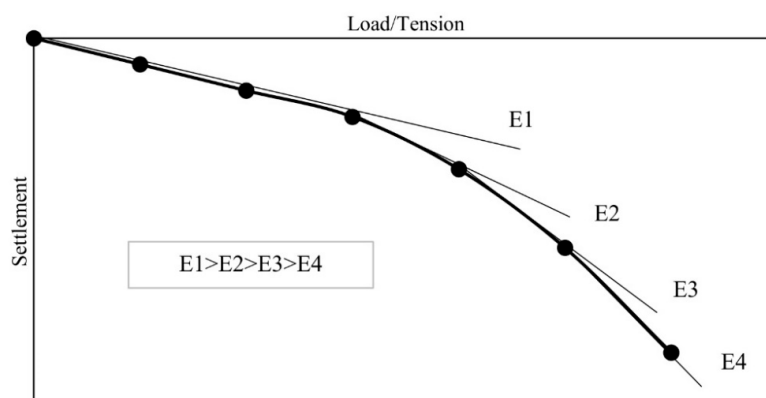


**Figure 1.** Typical load–settlement curve from a plate load test.

The excavation performed before the construction of mat foundations is another important factor in the development of settlements. Such removal may result in relaxed subgrade tension and, as a result, settling after recompression.

The relationship between the soil, the foundation, and the structure influences the performance of a building in a complex mechanism known as soil–structure interactions (SSIs). In spite of its importance, however, this connection is often overlooked and structural designs are still developed without taking into account this approach [34]. Determining the field monitoring settlement allows for an assessment of the building’s realistic performance, and important geotechnical factors may be studied [35,36].

More recently, foundation measurements [37–39] and analyses of soil–structure interaction modelling [40,41] have been investigated. These investigations have often been focused on framed buildings or industrial slabs [42]. In view of the limited availability of research on the behavior of concrete-walled constructions laid on a concrete mat foundation, the research developed and reported in this article seeks to contribute to the design strategies for this type of structure with qualitative and quantitative information from the examination of a real case.

### 1.2. Research Significance

This study discusses two important aspects that should be considered in the analysis and design of concrete-walled constructions on mat foundations: determining the appropriate modulus of elasticity for numerical simulations using measurements obtained from the field monitoring of settlements, and adopting a factor reduction modulus (FRM) dependent on the stress level in the foundation.

## 2. Materials and Methods

Thirteen of sixty-four apartment blocks in the city of São Lourenço da Mata (PE, Brazil) were analyzed. Eleven of the thirteen were built in landfill sections and two were built in land-cut sections. Figure 2 shows the project site. Each block had eight stories and 225 m<sup>2</sup> of space. The building technique consisted of concrete walls over mat foundations. The mats had thicknesses of 0.35 m and surface-mounted areas of 262 m<sup>2</sup>.

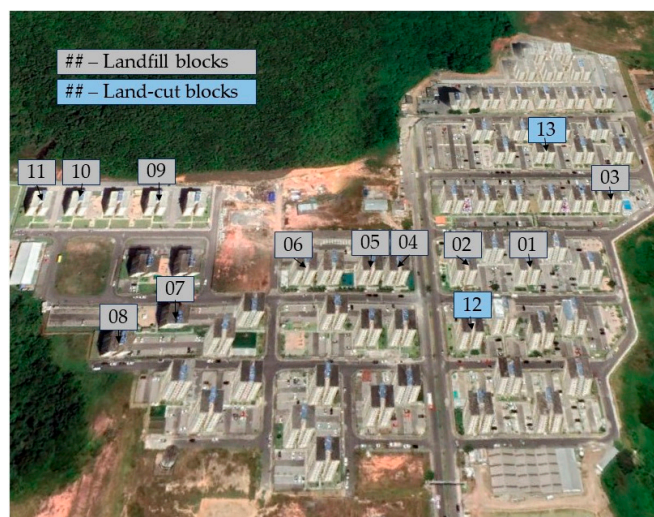


**Figure 2.** Project site (Image from Google Earth—8°01′30.6″ S 35°02′23.0″ W).

### 2.1. Geotechnical Investigation and Properties

For each building under consideration, two SPTs were performed per block (opposite sides) for a geotechnical investigation. No groundwater was observed. Table 1 exhibits the most prevalent soil types as well as the average blow count (average  $N_{SPT}$ —number of blows) for each soil unit, and Figure 3 shows typical soil profiles and the corresponding SPT value for Buildings 2, 4, and 5. In this figure, the depth is shown on the left and right sides in the geotechnical profile obtained for each block, where each marking corresponds to 1 m of prospecting and the number of blows obtained. The same color was used to represent the same soil in the figures shown. The main geotechnical information obtained from the

performed static penetration tests was the identification of the different soil layers that comprised the subsoil, the classification of the soils in each layer, and the water table level. The classification shown in the figures represents a pattern observed for the respective blocks and was as follows: medium-red and yellow, variegated clayey silt—at some depths, with the presence of mica–sandy silt (mica, medium compact pebbles of varying sizes, and fine, slightly silty sand).

**Table 1.** Geotechnical properties (earthmoving and  $N_{SPT}$ ).

Building	Section Type	Type of Soil	$N_{SPT}$	Standard Deviation	Coefficient of Variation (%)
1	Landfill	Clayed Silt	10	3.4	35
2	Landfill	Clayed Silt	9	3.3	38
3	Landfill	Clayed Silt	10	4.7	46
4	Landfill	Clayed-Sandy Silt	8	2.1	27
5	Landfill	Sandy Silt	10	2.5	26
6	Landfill	Clayed Silt	12	4.5	37
7	Landfill	Sandy Silt	14	4.8	35
8	Landfill	Clayed-Sandy Silt	10	3.9	40
9	Landfill	Clayed Silt	11	3.8	34
10	Landfill	Clayed Silt	9	3.7	41
11	Landfill	Clayed Silt	9	2.9	33
12	Land-cut	Silty Clay	10	2.4	25
13	Land-cut	Clayed Silt	9	4.6	46

The correlations of  $N_{SPT}$  and the elastic modulus are given by Equation (1), as suggested by Teixeira and Godoy [43].

$$E = \alpha \cdot \beta \cdot N_{SPT} (\text{MPa}) \quad (1)$$

where  $\alpha$  and  $\beta$  are coefficients that depend on the type of soil. Table 2 exhibits the coefficients  $\alpha$  and  $\beta$  as determined by Trofimenkov [29] and Teixeira [30], respectively.

**Table 2.** Coefficients  $\alpha$  and  $\beta$  as determined in [29,30].

(a) $\alpha$ Values		(b) $\beta$ Values	
Soil Type	$\alpha$ —Value	Soil Type	$\beta$ —Value
Sand	3	Sand with gravel	1.1
Silt	5	Sand	0.9
Clay	7	Silty sand	0.7
		Clayed sand	0.55
		Sandy silt	0.45
		Silt	0.35
		Sandy clay	0.3
		Clayed silt	0.25
		Silty clay	0.2

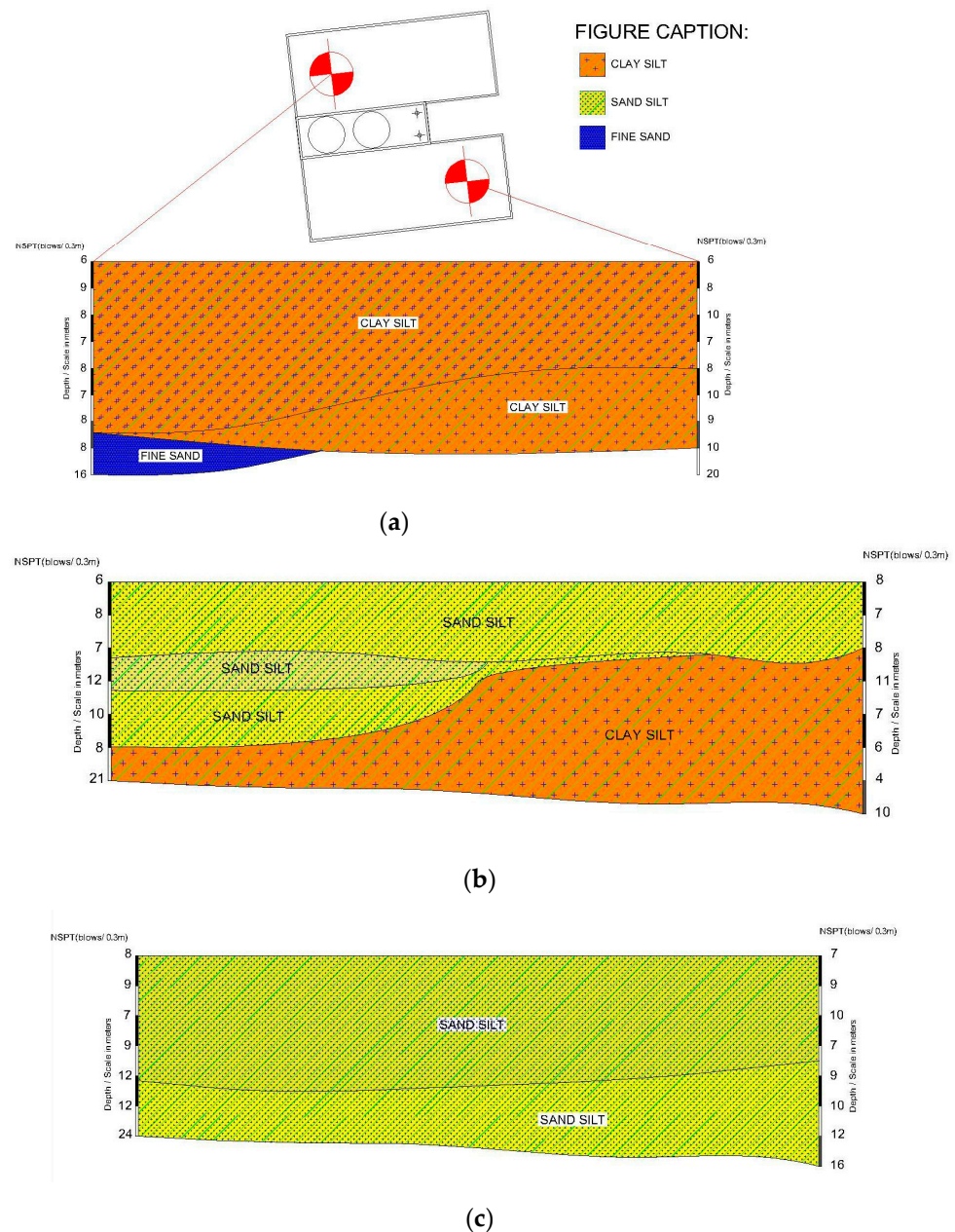


**Figure 3.** Typical soil profiles: (a) Building 2, (b) Building 4, and (c) Building 5.

The computer program ELPLA 10.1 Professional [44] from the GEOTEC v. 13.1 software was used to estimate the settlement by considering the assumption of a rigid concrete plate on an elastic foundation. ELPLA is a program for analyzing a raft of an arbitrary shape and a variable thickness and foundation depth, with three subsoil models available—the simple assumption model, the Winkler model, and the continuum model. The latter was used in this research. The mathematical solution of the raft was based on the FE method and the settlements were calculated for the bilinear deformation behavior of the soil, according to the theory of elasticity. Additional details on the use of the ELPLA program for the calculation of settlements and reinforcements throughout the research can be found in [45]. The soil was divided by the number of borings, with each one having multiple layers with different soil materials. The foundation soil was adopted as an elastic, linear, homogeneous, and isotropic material. The hypothesis of linear elastic behavior was justified because the settlements of the rigid plate measured in the field showed markedly linear behavior with the acting tension. The characteristics of the homogeneity and isotropy of the soil were

justified because the applied stress level was relatively low and, in this way, the material's response was very close to the response of an isotropic and homogeneous material. To determine the settlements and contact pressures, the modulus of compressibility method for the rigid raft was used. This method assumes that the raft is completely rigid, which means a raft with both its thickness and flexure rigidity tending to infinity.

The finite element mesh that defines the radier was created, measuring 16.50 m in the X and Y axes. A constant interval of 0.5 m was used in the two X and Y axes, thus forming a finite element grid with 1134 nodes (Figure 4a). The modulus of elasticity of the radier (concrete) was adopted at 20,000 MPa and a Poisson's coefficient of 0.15. After determining the representative mesh of the radier, the linear loads from the concrete walls were placed. The linear loads ranged from 77 to 176.4 kN/m (Figure 4a).

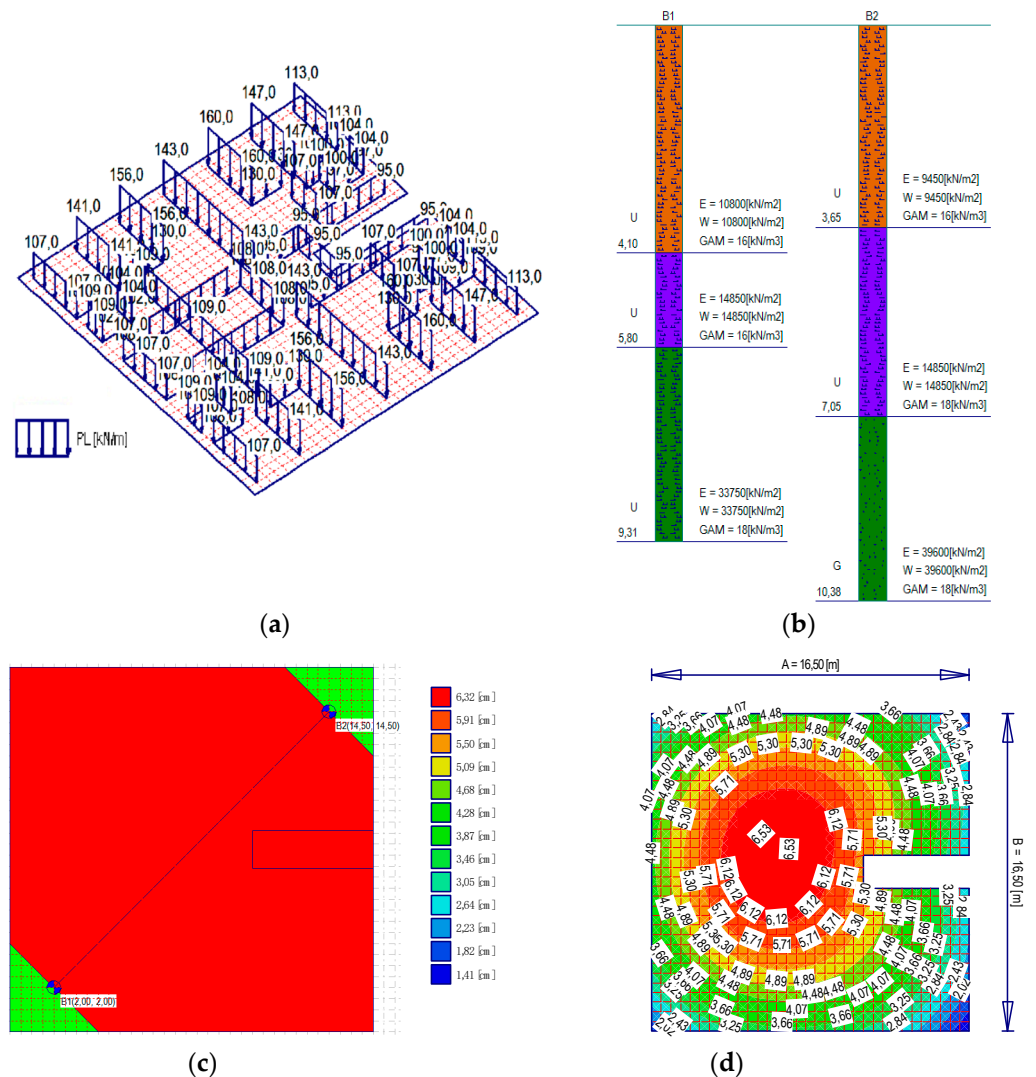


**Figure 4.** Developed ELPLA model: (a) FE mesh; (b) geotechnical profiles; (c) geotechnical profile interpolation; and (d) settlements calculated.

The option of inserting the parameters of the two boreholes was used and the location of the boreholes in relation to the studied radier was determined. The values of the modulus of elasticity, modulus of elasticity of recompression (W), and soil-specific weight (GAM) were assigned, as shown in Figure 4b. The method of interpolation of the properties of the inserted profiles was used to determine the geotechnical profile of the calculation (Figure 4c). The red color graphically represents the region where the profiles

were interpolated. After that, the program was used to calculate the settlement of the model, obtaining the settlements as shown in Figure 4d.

## 2.2. Estimated Loading

The concrete walls of the blocks under study on each floor were built in two stages. The first stage corresponded to the walls on the left and the central walls of the building. The second stage corresponded to the walls on the right side of the building. In this way, a standard methodology was indicated for the execution of the blocks, since the construction of the first part of the building (left and central walls) was generally assembled in one day and was cast at the end of that day. The next day, the right-side walls were assembled and cast at the end of the same day. This construction system was numerically simulated using the non-linear stage construction module of the SAP2000 v23.1.0 software [42], consisting of a total of 19 load cases, as follows:

- Construction of the foundation—Step 1;
- Construction of the left side and central walls of the first floor of the building—Step 2;
- Construction of the right walls of the first floor of the building—Step 3;
- Repeat Steps 2 and 3 for the 2nd to 17th floors of the building—Steps 4–17;
- Construction of the deck and elevated water tank—Steps 18–19.

Table 3 summarizes the estimated loads for each step and the expected foundation stresses.

**Table 3.** Loads for each step of the model and the expected foundation stresses (L—left walls; C—center walls; and R—right walls).

Step	Stage	Estimated Load (End of Step), kN	Expected Stress (End of Step), kPa
1	Foundation	2295	8.8
2	1L + 1C	3365	12.8
3	1R	4243	16.2
4	2L + 2C	5317	20.3
5	2R	6194	23.6
6	3L + 3C	7268	27.7
7	3R	8146	31.1
8	4L + 4C	9220	35.2
9	4R	10,097	38.5
10	5L + 5C	11,171	42.6
11	5R	12,049	46.0
12	6L + 6C	13,123	50.1
13	6R	14,000	53.4
14	7L + 7C	15,074	57.5
15	7R	15,952	60.9
16	8L + 8C	17,024	65.0
17	8R	17,902	68.3
18	Roof	18,315	69.9
19	Elevated water tank	18,619	71.1

## 2.3. Back-Analysis of the Foundation's Modulus of Elasticity

The elastic theory equation (Equation (2)) by Harr [17] was used to back-analyze the elastic modulus using the settlement data and the corresponding estimated loads.

$$E \text{ (MPa)} = \Delta q \text{ (MPa)} \cdot B \text{ (m)} \frac{1 - \nu^2}{\Delta w \text{ (m)}} I_s I_h \quad (2)$$

where  $E$  is the modulus of elasticity;  $\Delta q$  is the distributed expected stress;  $\Delta w$  is the average settlement considering the 10 readings taken;  $\nu$  is Poisson's ratio, which was considered equal to 0.3;  $I_s$  is a factor that depends on the shape and rigidity of the foundation; and  $I_h$  is a factor that depends on the foundation's depth.



Figure 5 shows the  $h/a$  relationship used to calculate  $I_s$  and  $I_h$ . In Figure 5,  $h$  represents the depth of the rigid base, defined as that at which the number of standard penetration tests ( $N_{SPT}$ ) was greater than 30, and  $a$  stands for the smallest dimension of the foundation (8.175 m). An  $N_{SPT}$  greater than 30 was considered because it was assumed that the stress level acting on the foundation was negligible for the settlements. Once the elevation of the rigid base was determined, it was possible to obtain the product of the corrective factors— $I_s \cdot I_h$ —for the foundation plate of each block analyzed in Figure 5b. Figure 5a illustrates the meaning of the  $h/a$  ratio.

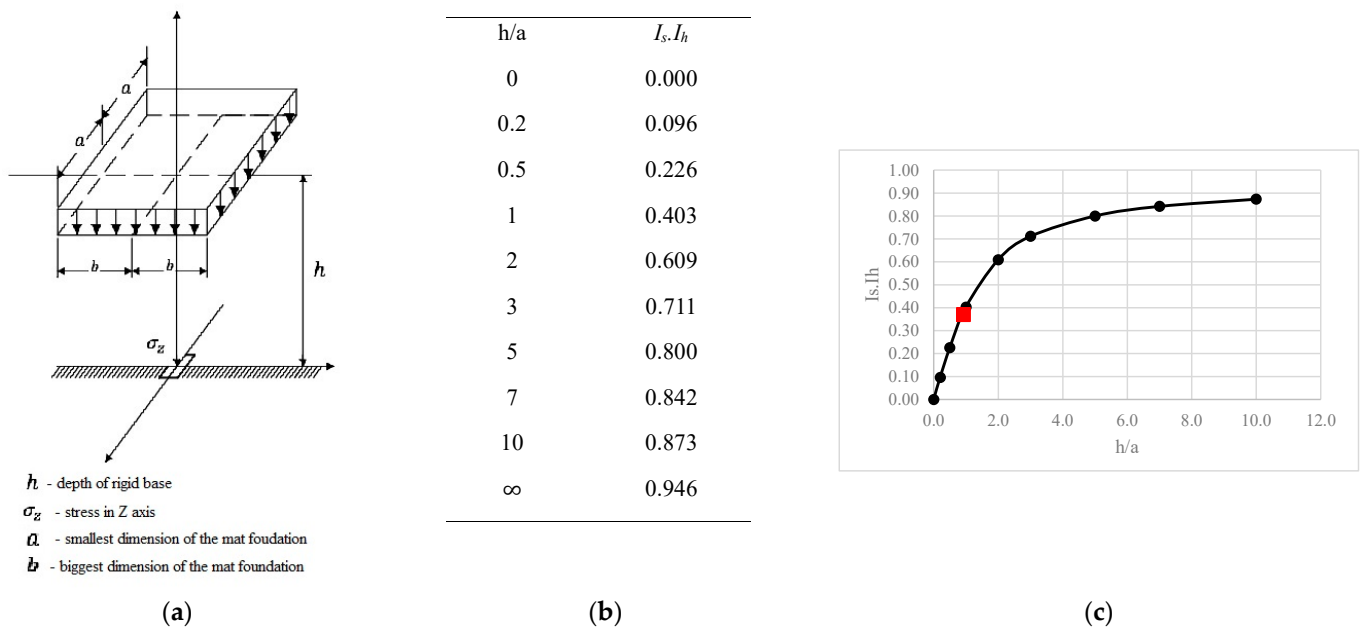


**Figure 5.** Parameters for obtaining corrective factors: (a) rigid depth dimension— $h$ , (b) product of  $I_s \cdot I_h$  for  $b/a = 1$  by Harr [17], and (c) interpolation process.

Equation (2) was formulated for the uniformly distributed stress. Since the loading resulting from the construction process only produced uniformly distributed normal stresses when all the walls were fully built on a respective floor, only at this stage were the settlement data analyzed.

The following is an example of the methodology used in order to make the adopted procedure more clear. The geotechnical profile's modulus of elasticity in Figure 3a was computed. Given the two geotechnical profiles, the average thickness of the stiff layer was 7.5 m, resulting in a ratio of 0.9  $h/a$  and a value of 0.37 for the product of  $I_s \cdot I_h$ . There was an increase in tension of 6.7 kPa and a settlement development of 1.761 mm during the constructive progress. To obtain a value of 0.37 for the product of  $I_s \cdot I_h$ , a linear interpolation was performed between the values of  $h/a$  ranging from 0.5 to 1, as shown in Figure 5c. The following is an example calculation:

$$E = 0.0067 \text{ (MPa)} \cdot 16.35 \text{ (m)} \frac{1 - 0.3^2}{0.001761 \text{ (m)}} \cdot 0.3 = 21 \text{ MPa}$$

#### 2.4. Constructive Method

On each floor, the concrete walls were built in two phases, with the first consisting of the formworks of the left walls (L) and the center formworks (C). The right side (R) of the formwork was the second stage (see Figure 6). As a result, a standard approach for presenting the structural sequence of the building under consideration was created. It was assumed in this approach that the formworks for the first portion (L+C) were mounted in a day and cast on the same day. The formwork for the second part (R) was constructed the

next day and cast later that day. Table 4 summarizes the steps of this constructive process, which was one source of the input data for the numerical modelling developed.

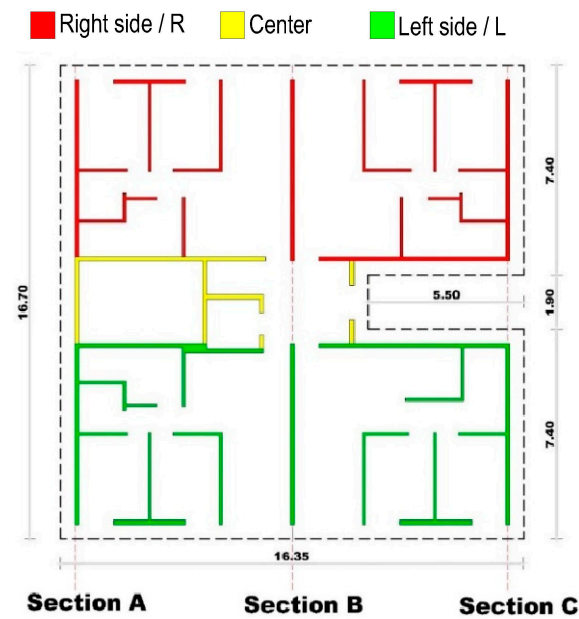


Figure 6. Stages of formworks.

Table 4. Constructive process phases.

Step	Stage	Executed Step
1	Foundation	Foundation construction
2	1L + 1C	Assembly of the left formwork of the 1st floor with the hall, elevator, and stairs, and casting at the end of the day
3	1R	Assembly of the right formwork of the ground floor and casting at the end of the day
4	2L + 2C	Assembly of the left formwork of the 1st floor, ground floor with hall, elevator, and stairs, and casting at the end of the day
5	2R	Assembly of the right formwork of the 1st floor and casting at the end of the day
6	3L + 3C	Assembly of the left formwork of the 2nd floor, ground floor with hall, elevator, and stairs, and casting at the end of the day
7	3R	Assembly of the right formwork of the 2nd floor and casting at the end of the day
8	4L + 4C	Assembly of the left formwork of the 3rd floor, ground floor with hall, elevator, and stairs, and casting at the end of the day
9	4R	Assembly of the right formwork of the 3rd floor and casting at the end of the day
10	5L + 5C	Assembly of the left formwork of the 4th floor, ground floor with hall, elevator, and stairs, and casting at the end of the day
11	5R	Assembly of the right formwork of the 4th floor and casting at the end of the day
12	6L + 6C	Assembly of the left formwork of the 5th floor, ground floor with hall, elevator, and stairs, and casting at the end of the day
13	6R	Assembly of the right formwork of the 5th floor and casting at the end of the day

Table 4. Cont.

Step	Stage	Executed Step
14	7L + 7C	Assembly of the left formwork of the 6th floor, ground floor with hall, elevator, and stairs, and casting at the end of the day
15	7R	Assembly of the right formwork of the 6th floor and casting at the end of the day
16	8L + 8C	Assembly of the left formwork of the 7th floor, ground floor with hall, elevator, and stairs, and casting at the end of the day
17	8R	Assembly of the right formwork of the 7th floor and casting at the end of the day
18	Roof	Roof assembly and casting
19	Elevated water tank	Water tank assembly and casting

### 2.5. Settlement Monitoring

Ten topographic monitoring pins were installed along the foundation to measure the displacement using optical equipment. Figure 7 shows the geometric dimensions of the foundation and the location of the anchor bolts, as well as the location of the concrete walls.

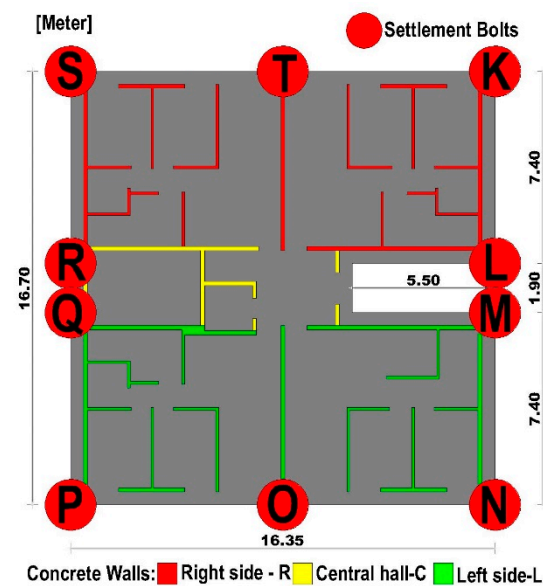
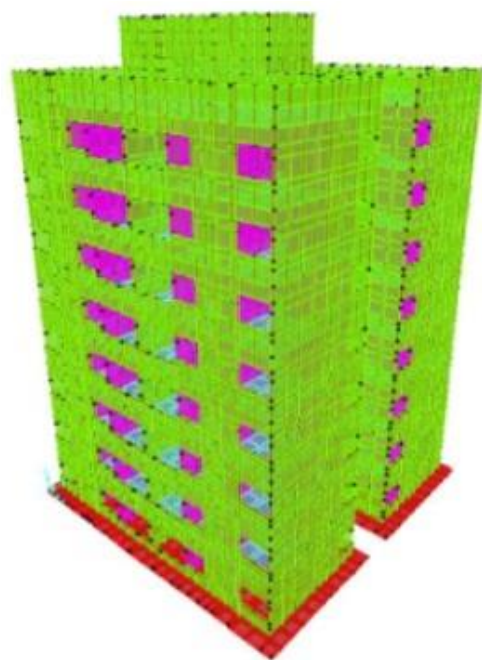


Figure 7. Mat foundations and locations of settlement bolts and concrete walls.

### 2.6. Numerical Model

Numerical models were developed using SAP2000, as shown in Figure 8. Table 5 summarizes the main information of the numerical model developed. The primary distinction between thin- and thick-shelled formulations was the incorporation of transverse shear deformation in plate-bending behavior. The thin-plate formulation was based on a Kirchhoff application, which ignores transverse shear deformation, whereas the thick-plate formulation was based on Mindlin/Reissner, which considers shear behavior. Only plate-bending (out-of-plane) behavior was affected by a thick-plate formulation, not membrane (in-plane) behavior.



**Figure 8.** A 3D model.

**Table 5.** Numerical model data.

Material	Unit Weight (kN/m <sup>3</sup> )	f'c (MPa)	$\nu$	E (GPa)	Element Type	Membrane Thickness (cm)	Bending Thickness (cm)
Foundation slab	25	35	0.2	33.13	Thick Plate	30/35	30/35
Floor slabs	25	25	0.2	28	Thin Plate	10	10
Walls, 15	25	25	0.2	28	Thin Shell	15	15
Walls, 10	25	25	0.2	28	Thin Shell	10	10

A structured rectangular finite element mesh was used to discretize the rigid foundation plate modeled. This was performed to make the process of calculating the tributary area of each node of the mesh easier for determining the associated spring constants.

The time-dependent properties of concrete—the evolution of the material's compressive strength and modulus of elasticity, creep, and shrinkage—were considered in the developed models, and the main parameters used followed the recommendations of CEB-FIP 90 [46]. Table 6 summarizes the data used to implement the time-dependent effects of the concrete.

**Table 6.** Time-dependent concrete parameters used.

Parameter	Value
Coefficient $\beta_{sc}$ —normal hardening cement	5
Coefficient $s$ —normal hardening cement	0.25
Aggregate type— $\alpha_E$	1.0
Age of concrete at the beginning of shrinkage— $t_s$ in days	0.0
Relative humidity of the ambient atmosphere (%)	50

The construction process was numerically simulated using an SAP2000 module called staged construction. Staged construction is a static modeling, analysis, and design application that enables the definition of a sequence of construction stages in which structural

systems and load patterns are added or removed and time-dependent behaviors are evaluated, including creep, shrinkage, and aging (change in elastic modulus and strengths with age). Material and geometric nonlinearity may be applied to staged construction. Further, staged construction may be part of a sequence of nonlinear static or direct-integration time-history analysis load cases. For linear load cases, the structural stiffness at a given construction stage may serve as the basis for analysis. Three different evaluation scenarios were investigated in the numerical modeling. The first scenario considered the modeling of construction stages as well as soil–structure interactions, and is referred to throughout the text as the acronym SSI-SC. In the second scenario, the modeling took into account the instantaneous application of the load in a single construction phase. In this scenario, the soil–structure interactions were also considered, but the effects of creep and shrinkage were not taken into consideration. This stage is referred to throughout the text as the acronym SSI-IL.

In the third case, the raft was modeled on an elastic basis with dispersed loads acting on it from the walls. This numerical model was dubbed the LRF (loaded raft foundation), and it dealt with the analysis by focusing just on the raft stiffness, without taking creep and shrinkage into account. In the third case, the rigid foundation slab was modeled as a slab on an elastic foundation. This numerical model is referred to as LRF. No creep or shrinkage effects were taken into account in this scenario. Figure 9 shows a graphical representation of the models analyzed.

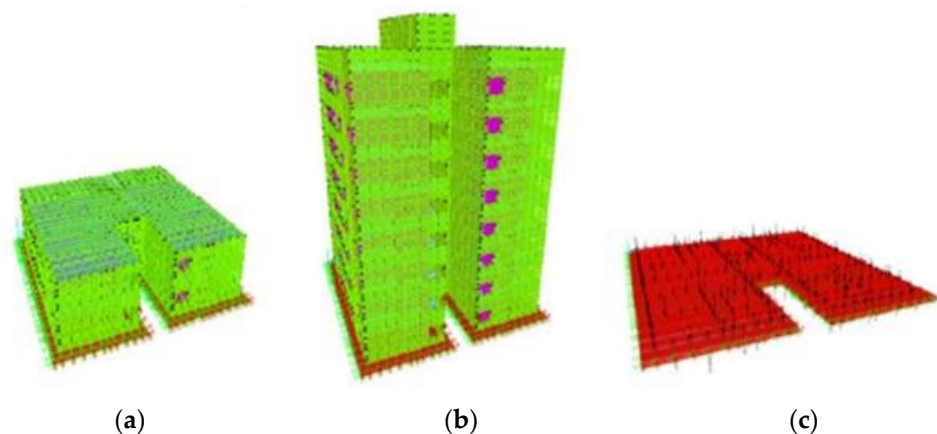


**Figure 9.** Graphical representation of the models analyzed: (a) SSI-SC, (b) SSI-IL and (c) LRF.

Figure 10 shows the geotechnical profile of the numerically investigated block. A profile with a silty-clay prevalence was identified, with an average  $N_{SPT}$  of 10 blows in a compressible layer ( $N_{SPT} > 30$  blows) of around 3 m following earthworks (land-cut sections).

The standard penetration test (SPT) is a widely used in situ geotechnical testing method employed to determine the subsurface soil properties. In this test, a hollow sampling tube is driven into the ground at the bottom of a borehole by a standard weight falling freely over a standard distance. The number of blows required for the sampler to penetrate each 150 mm (6-inch) interval is recorded. The SPT provides valuable information about soil resistance, which can be correlated with the soil type, density, and strength. Design engineers use the results of SPT tests to assess the soil's stability, bearing capacity, and settlement potential, aiding in the design and construction of foundations, retaining walls, and other geotechnical structures.

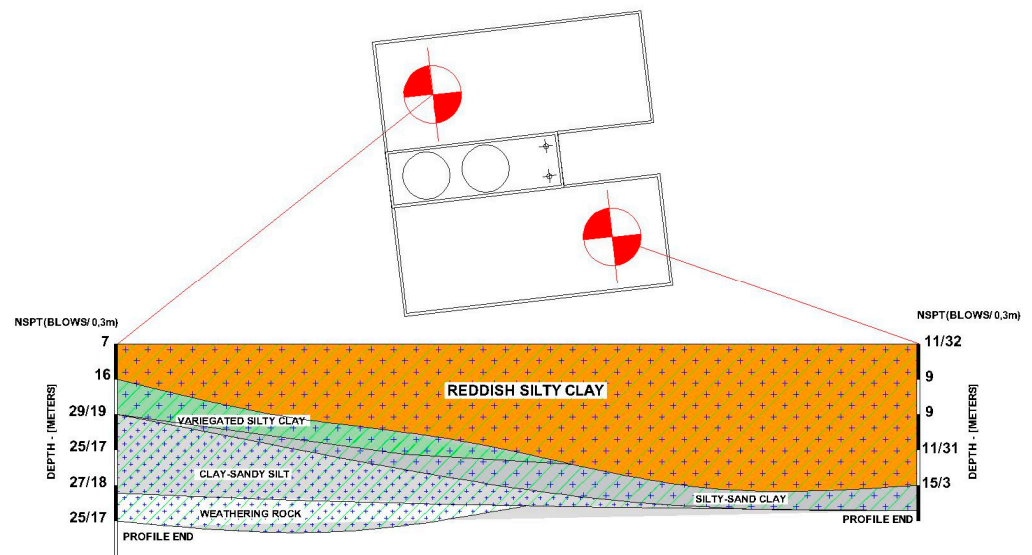


Figure 10. Geotechnical profile of subgrade.

To determine the values of the spring coefficients of the translation and rotation of the elastic foundation to be applied to the base nodes, the settlement data obtained in the retro-analyses of the modulus of elasticity were used to determine the volumetric reaction coefficient, according to Equation (3):

$$K \left( \frac{\text{kN}}{\text{m}^3} \right) = \frac{q \left( \frac{\text{kN}}{\text{m}^2} \right)}{w \left( \text{m} \right)} \tag{3}$$

where  $w$  is the average settlement measured in the 10 installed pins and  $q$  is the average vertical stress estimated at the time of measurement.

Once we had the volumetric coefficient of vertical reaction, the spring constants of translation and rotation were determined using tributary area concepts. Often, an assumption is made to calculate how much area of a plate can be attributed to a node or, in other words, the influence of each node on the surface area of a plate. It depends on the shape of the plate. For a perfect square or rectangular plate, each node will influence exactly  $\frac{1}{4}$  of the plate's surface area. But for a generalized quadrilateral, the best practice would be to calculate the center of the mass of the plate and then draw lines from that center point to the middle points of each side. The described tributary area calculation was the key procedure used internally by the commercial software to determine the linear spring constant. Figure 11 shows a generic tributary area of a finite element of the foundation plate slab.

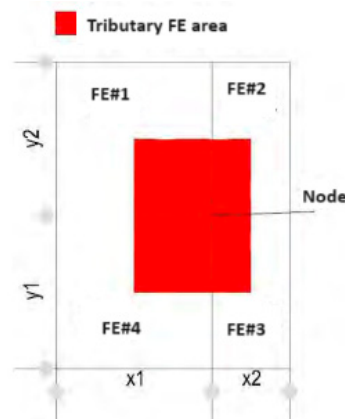


Figure 11. Generic tributary finite element area.

In this research, the tributary area for each node of the footing was first calculated, and then the modulus of the subgrade reaction was multiplied by the corresponding tributary area for each node to obtain the linear spring constants at each node. To calculate the rotation spring constants, the moment of inertia of the tributary areas was multiplied by the modulus of the subgrade. The linear springs in the direction of the U1 (X direction), U2 (Y direction), and U3 (Z direction) axes and the R1 (X direction) and R2 (Y direction) rotation springs are shown in Table 7.

**Table 7.** Linear and rotation spring constants.

Local Node Coordinates	Calculation Method
U1	U3 x Poisson's ratio
U2	U3 x Poisson's ratio
U3	Tributary area x modulus of subgrade
R1	"X" moment of inertia of tributary area x modulus of subgrade
R2	"Y" moment of inertia of tributary area x modulus of subgrade

This procedure was performed for each node that integrated the finite element model of the foundation. The Poisson's ratio of the soil that was used to calculate the spring constants in the X and Y directions was 0.3.

Based on the measurement of Building 02 (land-cut section) and the predicted vertical stress associated with numerical modelling, the settlement response coefficient obtained was 7900 kN/m<sup>3</sup>. This value was calculated from Equation (4) below [17].

$$K = \frac{E}{B \cdot (1 - \nu^2) \cdot I_s \cdot I_h} \quad (4)$$

where  $I_d$  is the layer-embedding factor. The other terms of the equation have already been qualified throughout the text, and their values were as follows:  $E = 18,800$  kN/m<sup>2</sup>,  $B = 16.5$  m,  $\nu = 0.3$ ,  $I_s \cdot I_h = 0.16$ , and  $I_d = 1$ —the value for the non-embedded layer, which is the case studied.

It is essential to point out that the settlements were measured at the raft foundation borders, which may have increased the settlement reaction coefficient, since the amount of deformation at the edge is less than that in the middle, depending on the global structural stiffness. Figure 12 exhibits a comparison of the average settlement observed at the plate's borders and the average settlement of the numerical model results.

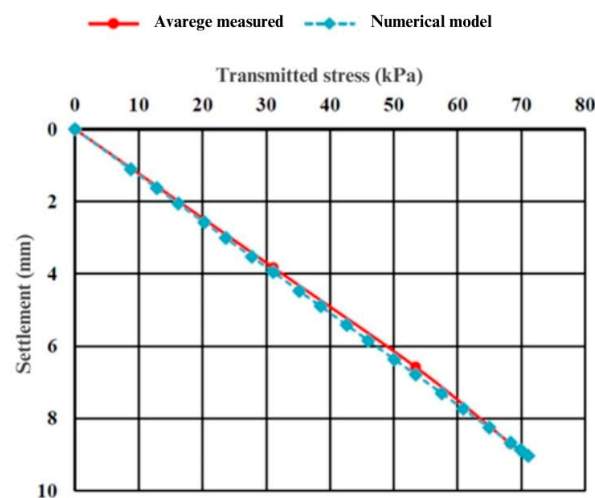


**Figure 12.** A comparative analysis of the average settlement measured at the edges of the plate and of the plate of the numerical model.

### 2.7. Soil–Structure Parameters

The absolute settlement factor (ASF) proposed by Gusmão [34] is given by Equation (5), which evaluates the settlement at a specific location in the raft by examining the connection between the settlement of this point ( $w_i$ ) and the average settlement ( $\bar{w}$ ) of all points.

$$ASF = \frac{w_i (\text{mm})}{\bar{w} (\text{mm})} \quad (5)$$

As a result, this value may be used to evaluate the foundation's load redistribution. When stress is relieved, the ASF parameter tends to drop, and when stress is increased, the ASF tends to increase.

The coefficient of variation (CV) is also often employed in foundation design evaluations of soil–structure interactions (SSIs). As indicated in Equation (6), it links the standard deviation ( $\sigma$ ) of the settlements obtained at the various measured points with the global average settlement.

$$CV = \frac{\sigma (\text{mm})}{\bar{w} (\text{mm})} \quad (6)$$

SSIs reduce the CV by distributing the load and, as a result, normalizing the settlements.

## 3. Results and Discussion

### 3.1. Modulus of Elasticity of Soils through Monitored Foundation Settlement

The results were separated into two groups based on the two possible scenarios: (a) mat foundations on landfill sections and (b) mat foundations over land-cut sections.

#### 3.1.1. Mat Foundations on Landfill Sections

The elastic modulus versus the predicted stress curves for mat foundations set over landfill sections are shown in Figure 13. At increased stresses, the elastic modulus was clearly reduced. Building 1's elastic modulus was reduced from 19.8 MPa to 8.8 MPa, while the stress increased by 23.3 kPa. With an estimated transmitted stress of 72.7 kPa, the soil beneath Building 4 presented the lowest back-analyzed elastic modulus value (1.1 MPa). Building 9's back-analyzed soil elastic modulus was reduced from 16 MPa to 8.4 MPa, while Building 5's value decreased from 13.1 MPa to 4.2 MPa.

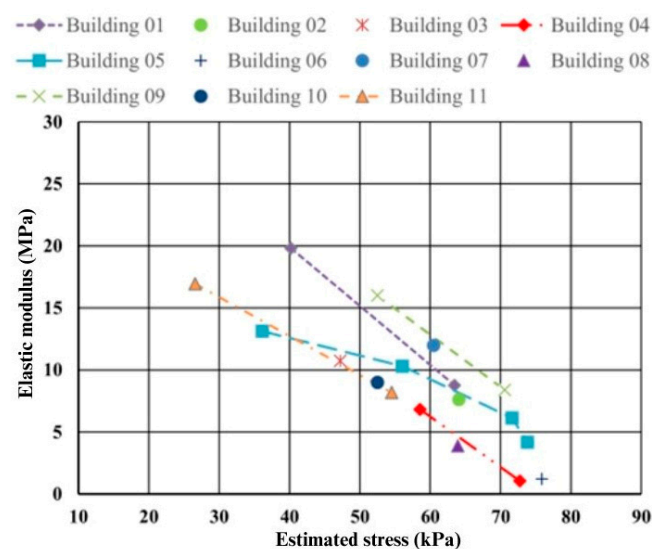


Figure 13. Elastic modulus versus estimated stress foundations on landfill sections.

This decrease in the elastic modulus showed that using constant deformability parameters for such a foundation might result in an underestimation of the expected settlement.



The above-mentioned data points were aggregated and interpolated by a single line to analyze the evolution of the elastic modulus variation as the load progressed (see Figure 8).

A polynomial equation (Equation (7)) defines the trend line with the best fit ( $R^2 = 0.71$ ) to the points, where  $E$  is the elastic modulus and  $\sigma_{est}$  is the transmitted estimated stress.

$$E \text{ (MPa)} = -0.0034\sigma_{est}^2 + 0.0508\sigma_{est} + 18.158 \quad (7)$$

Figure 14 shows that the development of the elastic modulus began at a value of about 17.5 MPa. The elastic modulus, determined using the Teixeira and Godoy [43] equation (Equation (2)) in a typical subsoil of structures constructed on landfill sections of silty soils with an average NSPT of 10, was the same as the value of the evolution curve. Mello's [28] recommended calculation (Equation (3)) yielded a slightly higher result of 21 MPa.

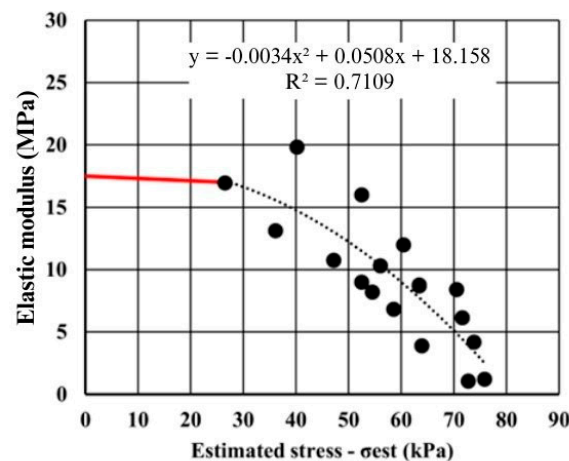


**Figure 14.** Evolution curve of back-analyzed elastic modulus for embankment earthmoving.

With this investigation, it can be shown that the modulus of elasticity started at a value close to those determined with the traditional equations. Then, as the transmitted stress increased, the modulus of elasticity decreased, suggesting a loss of rigidity in the subsurface layer. Table 8 shows a potential FRM that varied according to the stress level based on the back-analyzed elastic modulus evolution curve.

**Table 8.** Proposed factor-reduction modulus (FRM).

Transmitted Stress	FRM
<25 kPa	1.00
25 kPa < transmitted stress < 40 kPa	0.85
40 kPa < transmitted stress < 55 kPa	0.60
55 kPa < transmitted stress < 75 kPa	0.25

### 3.1.2. Mat Foundation on Land-Cut Sections

Figure 15 shows the elastic modulus versus the predicted stress curves for a mat foundation built over land-cut sections. The back-analyzed values of the soil elastic modulus decreased from 20.3 MPa to 17.4 MPa for Building 12, as well as from 19.4 MPa to 15.4 MPa for Building 13. The use of a constant elastic modulus for settlement predictions in the context of mat foundations over cuttings has demonstrated efficacy, as evidenced by minimal observed variation. This approach is particularly notable given the considerable heterogeneity documented in the literature regarding soil elastic moduli [17,26]. Notably, in the context of cut sections of land, this heterogeneity leads to pre-consolidation stresses, with the applied stress increments remaining below 80 kPa.

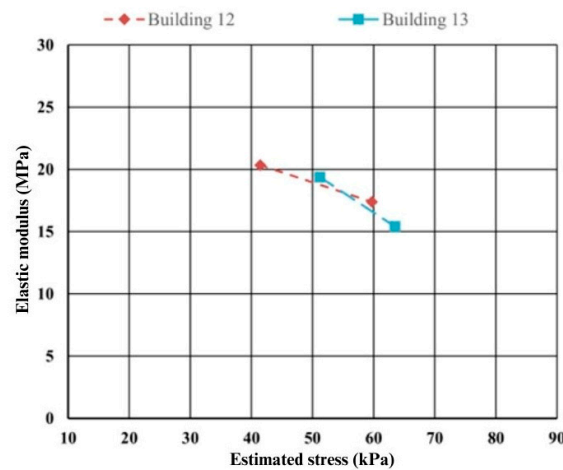


Figure 15. Elastic modulus versus estimated stress foundations on cut land.

### 3.1.3. Comparative Analyses of Settlement Monitoring

Figure 16 shows the measured and estimated settlement with ELPLA software for Buildings 1 and 2 (landfill sections—Figure 16a,b) and Buildings 12 and 13 (land-cut sections—Figure 16c,d). The FRM specified in Table 6 was used for landfill-section buildings, whereas the constant elastic modulus was used for land-cut sections. The use of the FRM in the prediction of settlement in landfill sections, with the ELPLA technique for settlement monitoring, is recommended.

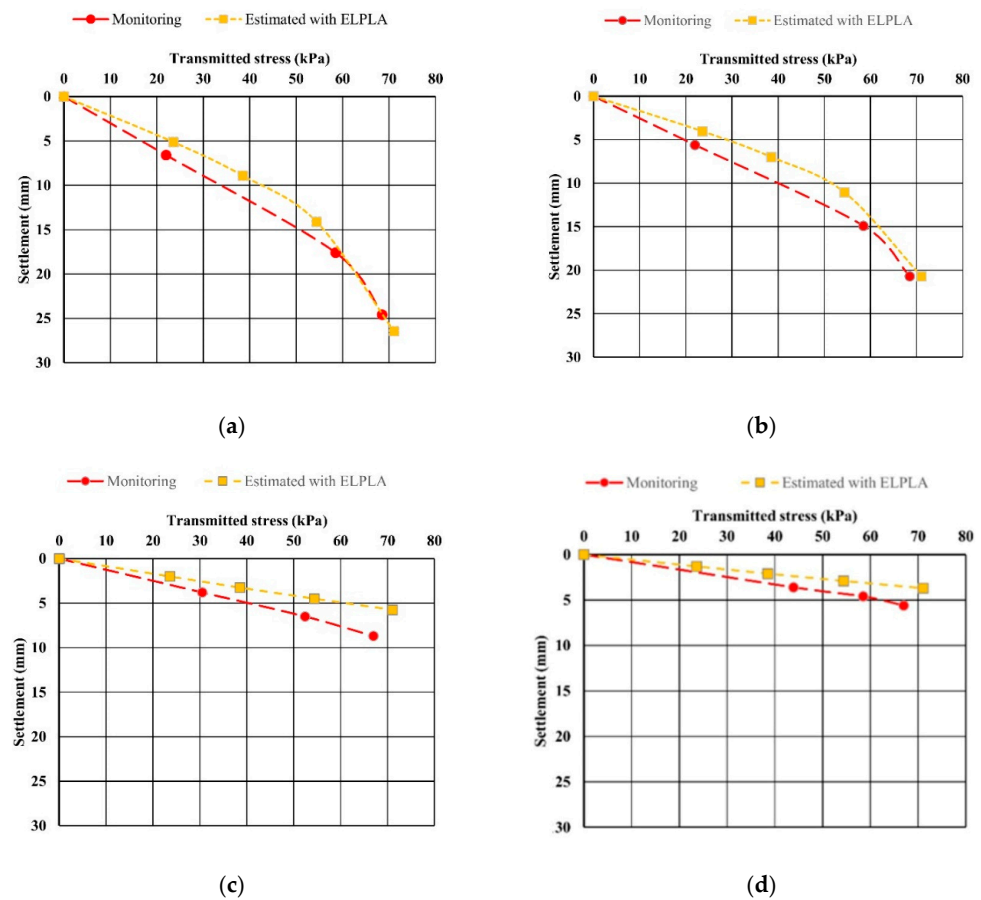


Figure 16. Comparative analyses of monitored settlement of (a) Building 1, (b) Building 2, (c) Building 12, and (d) Building 13.

### 3.2. Soil–Structure Interaction Analysis for a Concrete-Walled Building

The SSI attributes investigated were the effects of the constructive strategy on settlement uniformization and the influence of SSIs on stress development in concrete walls.

#### 3.2.1. Analysis of Soil–Structure Interaction Parameters

The minimum, average, and maximum settlements, as well as the standard deviations and coefficients of variation, were compared as a first assessment of the numerical models presented. The settlements included in this research were those associated with the general execution of the building in question.

Table 9 shows the data for the SSI-SC, SSI-IL, and LRF models. When compared to the LRF model, the SSI-SC model exhibited less variance between the minimum and maximum settlement, with the CV ranging from 4.07% to 5.20% for the SSI-SC model and 5.72% to 18.70% for the LRF model.

Since the loads imposed on the foundation in the last load stage were the same, the average settlement values observed in the numerical models were also the same. What stood out was the effect of the SSIs on the distribution of the vertical loads on the raft foundation and the consequent uniformity of the settlements. In the SSI-SC model, the coefficients of variation tended to be constant values, showing that the execution of the first floor already imposed a significant rigidity to the structure (foundation + superstructure). In the LRF model, the values for the coefficients of variation tended to increase with an increase in the loads. Figure 17 shows a comparative analysis of the coefficients of variation of the three models studied.

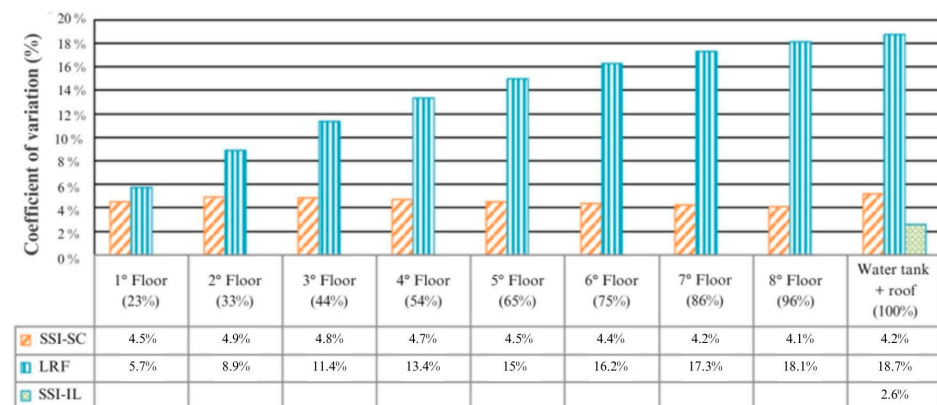


Figure 17. Comparative analysis of coefficients of variation.

Figure 18 exhibits the absolute settlement factor variations for the SSI-SC and LRF models. It demonstrates that the ASF for the SSI-SC model tended to have stable maximum and minimum values, but in the LRF model, the maximum factors tended to grow and the minimum factors tended to decline.

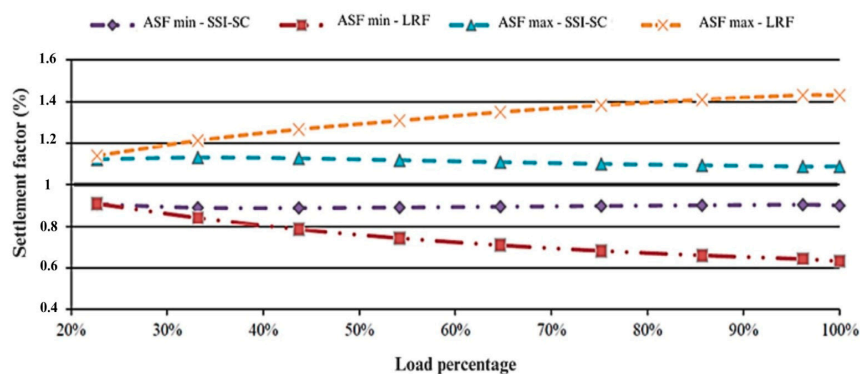


Figure 18. Variations in absolute settlement factor.

**Table 9.** Settlements for the scenarios investigated.

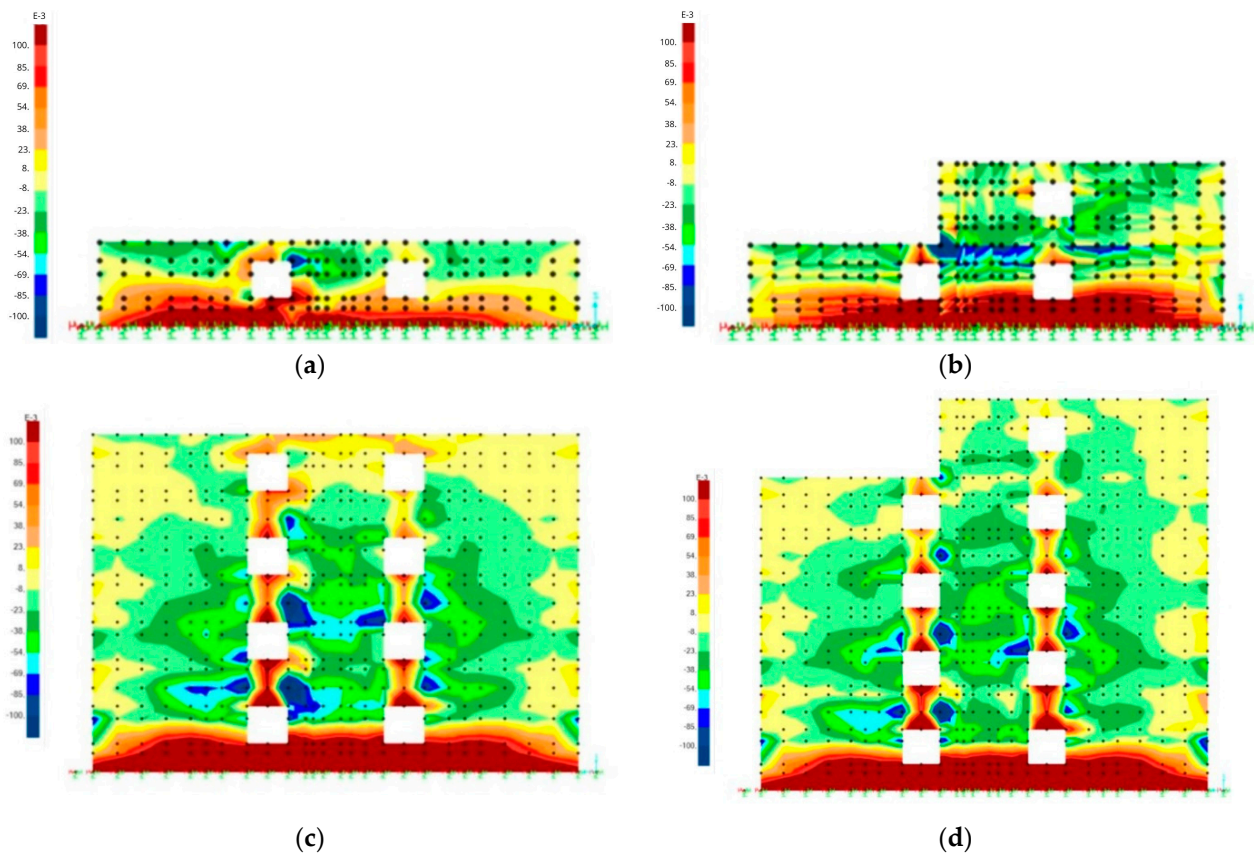
Step	Data	SSI-SC	LRF	SSI-IL
Fully Executed	$\omega_{avg}$ (mm)	9.04	9.15	9.01
	$\omega_{max}$ (mm)	9.83	13.08	9.46
	$\omega_{min}$ (mm)	8.13	5.77	8.54
	CV	5.20%	18.70%	2.56%
8th Floor	$\omega_{avg}$ (mm)	8.68	8.79	
	$\omega_{max}$ (mm)	9.44	12.57	
	$\omega_{min}$ (mm)	7.84	5.64	
	CV	4.10%	18.12%	
7th Floor	$\omega_{avg}$ (mm)	7.74	7.82	
	$\omega_{max}$ (mm)	8.46	11.02	
	$\omega_{min}$ (mm)	6.97	5.16	
	CV	4.22%	17.29%	
6th Floor	$\omega_{avg}$ (mm)	6.79	6.86	
	$\omega_{max}$ (mm)	7.47	9.48	
	$\omega_{min}$ (mm)	6.10	4.67	
	CV	4.36%	16.25%	
5th Floor	$\omega_{avg}$ (mm)	5.85	5.90	
	$\omega_{max}$ (mm)	6.48	7.96	
	$\omega_{min}$ (mm)	5.23	4.18	
	CV	4.52%	14.96%	
4th Floor	$\omega_{avg}$ (mm)	4.90	4.94	
	$\omega_{max}$ (mm)	5.48	6.46	
	$\omega_{min}$ (mm)	4.36	3.66	
	CV	4.69%	13.35%	
3rd Floor	$\omega_{avg}$ (mm)	3.95	3.98	
	$\omega_{max}$ (mm)	4.45	5.03	
	$\omega_{min}$ (mm)	3.51	3.12	
	CV	4.85%	11.36%	
2nd Floor	$\omega_{avg}$ (mm)	3.01	3.02	
	$\omega_{max}$ (mm)	3.40	3.66	
	$\omega_{min}$ (mm)	2.67	2.53	
	CV	4.07%	8.89%	
1st Floor	$\omega_{avg}$ (mm)	2.06	2.06	
	$\omega_{max}$ (mm)	2.31	2.35	
	$\omega_{min}$ (mm)	1.86	1.87	
	CV	4.49%	5.72%	

### 3.2.2. Influence of Soil–Structure Iterations on Wall Stresses

In order to analyze the combined action of construction effects and soil–structure interactions on the distribution of normal stresses in the wall, which is relevant information for the structural design of concrete building walls, three sections were chosen to graphically evaluate the redistribution of maximum normal stresses.

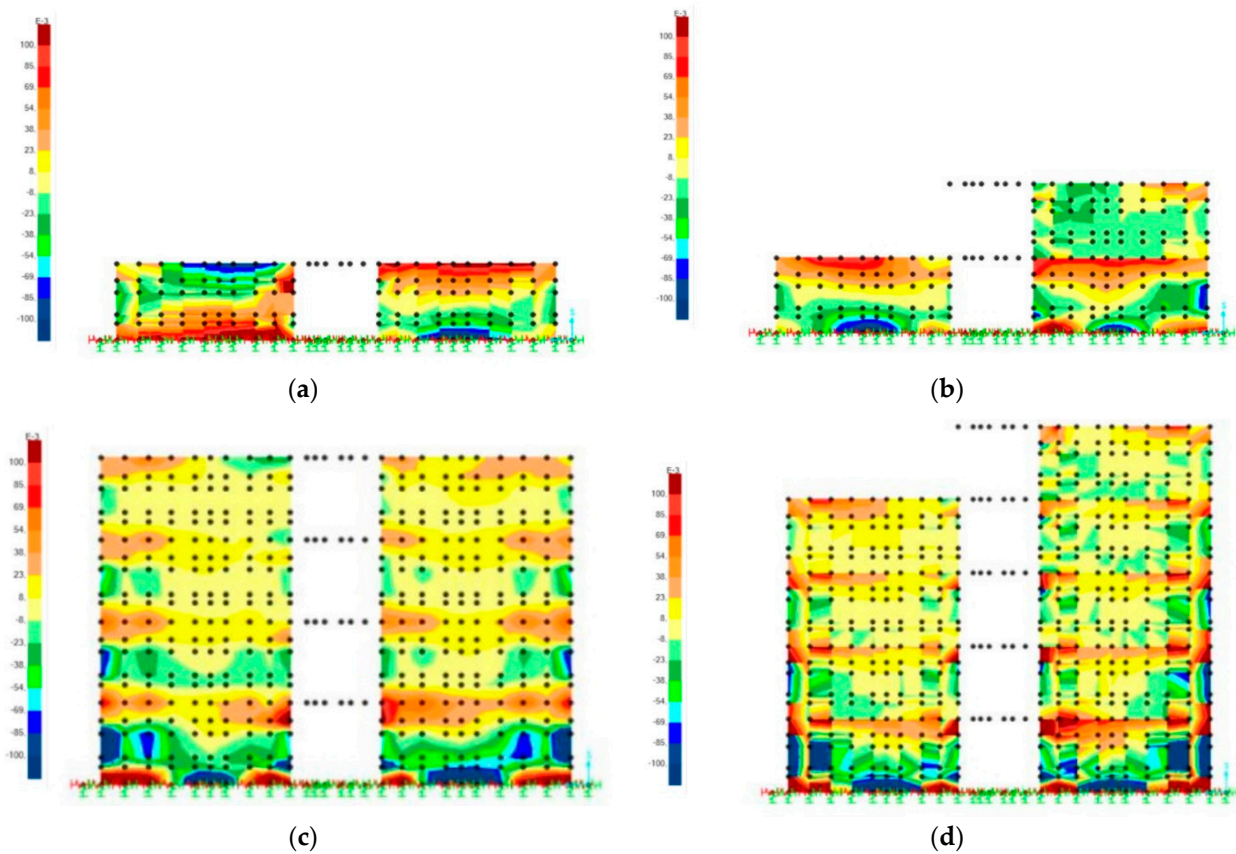
The chosen sections are shown in Figure 7, with Sections A and C consisting of exterior walls and Section B consisting of interior walls. Stage 4 (first floor) and Stage 5 (second floor, partially executed), as well as Stage 9 (fourth floor, complete) and Stage 10 (fifth floor, partially executed), were examined.

Figure 19a–d exhibit the maximum stress at Section A for Stages 4, 5, 9, and 10, respectively. The highest stress was found to be more concentrated close to the base of the walls on the right side in Stage 4. Normal maximum stress occurred on the opposite side to that observed without the complete execution of the upper floor, corresponding to Stage 5. When Stages 9 and 10 were examined, it was found that the maximum normal stress in the base of the walls did not tend to shift position. Normal stresses on the walls increased on the levels below the wall and in the region opposite the wall, illustrating the redistribution of stresses caused by the structure's stiffness.



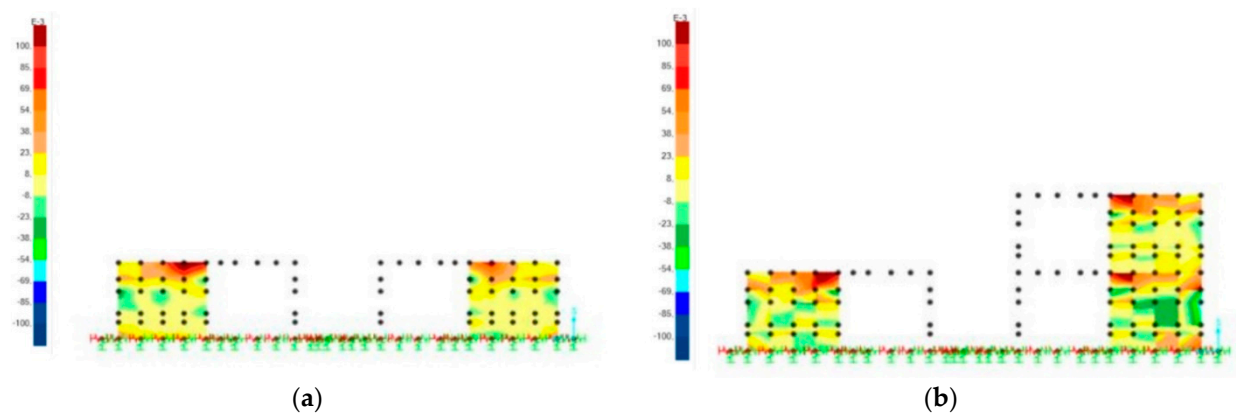
**Figure 19.** Analysis of maximum normal stresses in Section A for (a) Stage 4, (b) Stage 5, (c) Stage 9, and (d) Stage 10 (note:  $\text{kN}/\text{cm}^2$  is the unit of measurement).

Figure 20a–d show the maximum stress analysis in Section B for Stages 4, 5, 9, and 10, respectively. In Stage 4, the normal maximum compression stress occurred at the base of the walls on the right side, while normal tensile stress arose at the base of the walls on the left side. The highest normal tensile stress developed on the opposite side with the partial execution of the upper floor, corresponding to Stage 5 and demonstrating the foundation's lifting tendency. Normal maximum stresses at the base of the walls did not tend to shift position or direction (tension and compression) when Stages 9 and 10 were examined. There was an increase in the normal stresses in the walls on the floors below the wall and in the region opposite the wall, indicating load redistribution due to the stiffness of the structure. The SSI investigation of the construction stages affected the distribution of loads on various walls, an issue that is often overlooked in current concrete-walled construction projects. The observed behavior emphasizes the importance of considering the loads imposed on structures as a result of their construction process.



**Figure 20.** Analysis of maximum normal efforts in Section B for (a) Stage 4, (b) Stage 5, (c) Stage 9, and (d) Stage 10.

The maximum stress analysis for Section C in Stages 4, 5, 9, and 10 is shown in Figure 21a–d. The load development patterns were identical to those previously analyzed in Section A. It was observed that, in Stage 4, the maximum loads were more concentrated at the base of the walls on the observer's right; however, in Stage 5, the highest normal loads were concentrated on the opposite side to that observed previously. By analyzing Stages 9 and 10, it was observed that there was no significant distribution of stress in the walls opposite the load by the partial implementation of the floor, due to the discontinuity of the structure in the section under consideration.



**Figure 21.** *Cont.*

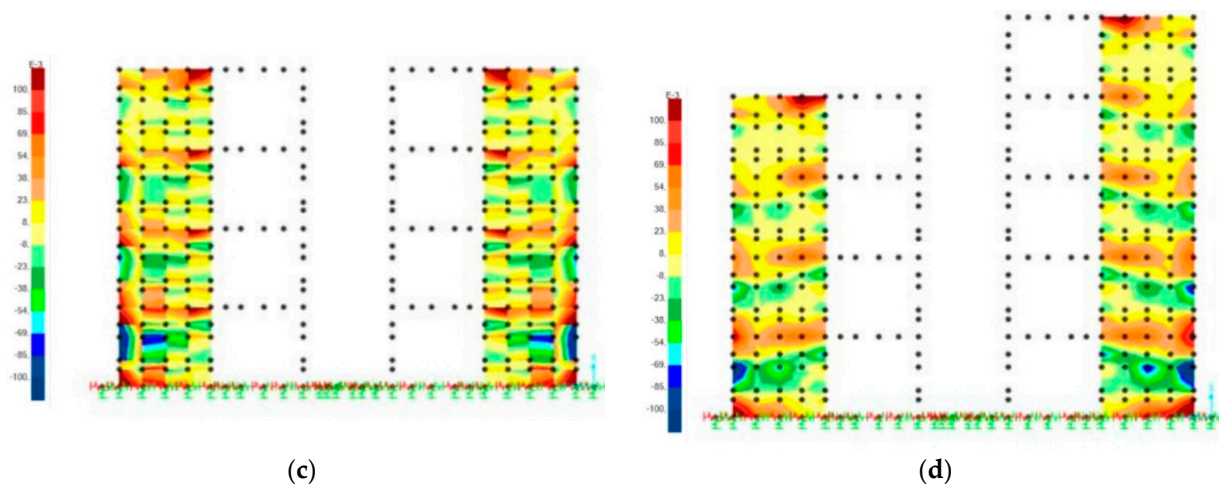


**Figure 21.** Analysis of maximum normal efforts in Section C for (a) Stage 4, (b) Stage 5, (c) Stage 9, and (d) Stage 10.

#### 4. Conclusions

The elastic modulus back-analysis has been significantly affected by earthmoving activities—landfill sections are more vulnerable to rigidity loss than land-cut sections. An analysis of mat foundations over landfill sections revealed that, as construction developed, the subsoil stiffness decreased, as measured by a reduction in the elastic modulus with an increase in the estimated transmitted stress. A proposed factor-reduction modulus (FRM), obtained from the back-analyzed elastic modulus development curve, was correlated with the transmitted stress levels of the mat foundations. This fact could be useful in predicting settlements in the type of construction under investigation.

The understanding of concrete raft foundations for structures with concrete walls can be improved by combining a soil–structure interaction (SSI) analysis with construction-stage consideration. This method can provide insight about the foundation behavior by highlighting the important influences of the superstructure and construction stages.

The superstructure and construction stages have a significant influence on the behavior of raft foundations, contradicting a common design assumption that ignores these aspects. This study highlighted that ignoring these aspects in the design of concrete raft foundations for structures with concrete walls might result in considerable discrepancies between the predicted and actual structural behavior under field conditions.

The results using the SSI-SC numerical model confirmed that taking construction stages into account is crucial for making accurate predictions about structural behavior, highlighting the importance of a uniform settlement pattern and reduced partial execution distortions. Based on the results obtained, the authors strongly recommend that the simultaneous consideration of soil–structure interactions as well as the construction effects be commonly used in foundation designs.

Lines of research that include the consideration of settlement velocity as well as the definition of performance parameters for concrete-walled constructions over raft foundations are relevant research topics.

**Author Contributions:** All the authors contributed to the development, analysis, writing, and revisions of this paper; conceptualization, F.A.N.S., J.D.P. and A.D.G.; methodology, S.R.M.F., F.A.N.S., J.D.P. and A.D.G.; software, S.R.M.F. and F.A.N.S.; validation, F.A.N.S., H.J.K. and J.M.P.Q.D.; formal analysis, F.A.N.S., H.J.K., J.M.P.Q.D. and A.C.A.; investigation, S.R.M.F., F.A.N.S., J.D.P. and A.D.G.; writing—original draft preparation, S.R.M.F. and F.A.N.S.; writing—review and editing, F.A.N.S., J.M.P.Q.D., H.J.K. and A.C.A.; visualization, F.A.N.S., H.J.K. and J.M.P.Q.D.; supervision, F.A.N.S., J.D.P. and A.D.G.; funding acquisition, F.A.N.S. and J.M.P.Q.D. All authors have read and agreed to the published version of the manuscript.

**Funding:** This work was financially supported by national funds through the FCT/MCTES (PIDDAC), under the project 2022.06841.PTDC—BlueHouseSim—Development of numerical simulation tools and methodologies for high-efficiency off-the-electrical-grid houses, with a DOI of 10.54499/2022.06841.PTDC (<https://doi.org/10.54499/2022.06841.PTDC>). In addition, this work was financially supported by Base Funding—UIDB/04708/2020, with a DOI of 10.54499/UIDB/04708/2020 (<https://doi.org/10.54499/UIDB/04708/2020>); Programmatic Funding—UIDP/04708/2020, with a DOI of 10.54499/UIDP/04708/2020 (<https://doi.org/10.54499/UIDP/04708/2020>) of the CONSTRUCT funded by national funds through the FCT/MCTES (PIDDAC); and FCT through the individual Scientific Employment Stimulus 2020.00828.CEECIND/CP1590/CT0004—DOI of 10.54499/2020.00828.CEECIND/CP1590/CT0004 (<https://doi.org/10.54499/2020.00828.CEECIND/CP1590/CT0004>). Finally, the authors express their gratitude to CNPq for providing finances and Gusmão Engenheiros Associados Ltda, who provided the data for analysis.

**Data Availability Statement:** The data that support the findings of this study are available from the authors upon request.

**Conflicts of Interest:** The authors declare no conflicts of interest.

## References

- Zhang, Y.; Cai, X.D.; Liu, R.; Xie, H.T.; Yi, Y.J. Seismic behavior of reinforced concrete frame substructure with cast-in-place slab on independent foundation. *Soil Dyn. Earthq. Eng.* **2022**, *157*, 107255. [[CrossRef](#)]
- Bennett, V.; Abdoun, T.; Zeghal, M.; Koelewijn, A.; Barendse, M.; Dobry, R. Real-Time Monitoring System and Advanced Characterization Technique for Civil Infrastructure Health Monitoring. *Adv. Civ. Eng.* **2011**, *2011*, 870383. [[CrossRef](#)]
- Zhu, C.; Zhang, L.; Liao, C.; Wei, X.; Ye, G. Estimation of horizontal bearing capacity of mat foundation on structured and over-consolidated clays under cyclic wave loads. *Soil Dyn. Earthq. Eng.* **2022**, *161*, 107426. [[CrossRef](#)]
- Asli, C.; Feng, Z.-Q.; Porcher, G.; Rincint, J.-J. Back-calculation of elastic modulus of soil and subgrade from portable falling weight deflectometer measurements. *Eng. Struct.* **2012**, *34*, 1–7. [[CrossRef](#)]
- Farias, R.S. Structural Analysis of Concrete Wall Buildings Including Soil-Structure Interaction and Progressive Loading. Ph.D. Thesis, Escola de Engenharia de São Carlos, São Carlos, Brazil, 2018.
- González-Arteaga, J.; Alonso, J.; Moya, M.; Merlo, O.; Navarro, V.; Yustres, Á. Long-term monitoring of the distribution of a building's settlements: Sectorization and study of the underlying factors. *Eng. Struct.* **2020**, *205*, 110111. [[CrossRef](#)]
- Zhussupbekov, A.; Tanyrbergenova, G.; Omarov, A. Design of anchored diaphragm wall for deep excavation. *Int. J. Geomate* **2019**, *16*, 139–144. [[CrossRef](#)]
- Bapir, B.; Abrahamczyk, L.; Wichtmann, T.; Prada-Sarmiento, L.F. Soil-structure interaction: A state-of-the-art review of modeling techniques and studies on seismic response of building structures. *Front. Built Environ.* **2023**, *9*, 1120351. [[CrossRef](#)]
- Santos, Y.R.P.; Bello, M.I.M.C.V.; Gusmão, A.D.; Patricio, J.D. Soil-structure interaction analysis in reinforced concrete structures on footing foundation. *Soils Rocks* **2021**, *44*, 1–12. [[CrossRef](#)]
- Alnmr, A.; Alsirawan, R. Numerical Study of the Effect of the Shape and Area of Shallow Foundations on the Bearing Capacity of Sandy Soils. *Acta Polytech. Hung.* **2024**, *21*, 103–120. [[CrossRef](#)]
- Alnmr, A.; Sheble, A.; Ray, R.; Ahmad, H. Parametric Investigation of Interaction between Soil-Surface Structure and Twin Tunnel Excavation: A Comprehensive 2D Numerical Study. *Infrastructures* **2023**, *8*, 124. [[CrossRef](#)]
- Poulos, H.G. Analysis of Foundation Settlement Interaction among Multiple High-Rise Buildings. *Geotech. Geol. Eng.* **2023**, *41*, 2815–2831. [[CrossRef](#)]
- Ertürk Atmaca, E.; Genç, A.F.; Altunişik, A.C.; Günaydin, M.; Sevim, B. Numerical Simulation of Severe Damage to a Historical Masonry Building by Soil Settlement. *Buildings* **2023**, *13*, 1973. [[CrossRef](#)]
- Stewart, J.P.; Murphy, D.; Largent, M.; Curran, H.; Egan, J.A. Foundation Settlement and Tilt of Millennium Tower in San Francisco, California. *J. Geotech. Geoenviron. Eng.* **2023**, *149*, 1–22. Available online: <https://ascelibrary.org/doi/epdf/10.1061/JGGEFK.GTENG-10244> (accessed on 5 March 2024). [[CrossRef](#)]
- Ng, S.-C.; Low, K.-S.; Tioh, N.-H. Newspaper sandwiched aerated lightweight concrete wall panels - Thermal inertia, transient thermal behavior and surface temperature prediction. *Energy Build.* **2011**, *43*, 1636–1645. [[CrossRef](#)]
- Loukidis, D.; Tamiolakis, G.P. Spatial distribution of Winkler spring stiffness for rectangular mat foundation analysis. *Eng. Struct.* **2017**, *153*, 443–459. [[CrossRef](#)]
- Harr, M.E. *Foundations of Theoretical Soil Mechanics*; MC Graw-Hill, Inc.: New York, NY, USA, 1996.
- Giroud, J.P. *Tables Pour le Calcul des Fondations*; Dunod: Paris, France, 1972.
- Poulos, H.G.; Davis, E.H. *Elastic Solutions for Soil and Rock Mechanics*; John Wiley and Sons: New York, NY, USA, 1974.
- Perloff, W.H. Pressure distribution and settlements. In *Foundation Engineering Handbook*; Winterkorn, H.F., Fang, H., Eds.; Van Nostrand Reinhold Company: New York, NY, USA, 1975.
- Padfield, C.J.; Sharrock, M.J. *Settlement of Structures on Clay Soils*; CIRIA Special Publication 27/PSA Civil Engineering Technical Guide 38; Department of the Environment: London, UK, 1983.



22. U.S. Army Corps of Engineers. *Engineering Manual—Settlement Analysis*; Publication EM 1110-2-1904; USACE: Washington, DC, USA, 1994.
23. Das, B.M. *Shallow Foundations: Bearing Capacity and Settlement*, 3rd ed.; CRC Press, Taylor and Francis Group: Boca Raton, FL, USA, 2017.
24. Fellenius, B.H. Pile foundations. In *Foundations Engineering Handbook*; Fang, H.Y., Ed.; Springer: Berlin/Heidelberg, Germany, 1991; pp. 511–536.
25. Sherif, G.; Konig, G. *Raft and Beams on Compressible Subsoil*; Springer: Berlin/Heidelberg, Germany, 1975.
26. Bowles, J.E. *Foundation Analyses and Design*; MC Graw-Hill, Inc.: New York, NY, USA, 1977.
27. Terzaghi, K.; Peck, R.B. *Soil Mechanics in Engineering Practice*; John Wiley & Sons: New York, NY, USA, 1948.
28. Mello, V.F.B. The Standard Penetration Test. In Proceedings of the IV Panamerican Conference on Soil Mechanics and Foundation Engineering, San Juan, PR, USA, 19–25 June 1971; American Society of Civil Engineers: New York, NY, USA, 1971; Volume 1, pp. 1–86.
29. Trofimenkov, J.G. Penetration testing in Eastern Europe. In Proceedings of the European Symposium on Penetration Resistance, Stockholm, Sweden, 5–7 June 1974; Volume 2.1, pp. 24–28.
30. Teixeira, A.H. An improvement in simple percussion recognition surveys. In *Solos do Interior de São Paulo*; ABMS: São Carlos, Brazil, 1993; Chapter 4.
31. Sharma, L.K.; Singh, R.; Umrao, R.K.; Singh, T.N. Evaluating the modulus of elasticity of soil using soft computing system. *Eng. Comput.* **2016**, *33*, 497–507. [[CrossRef](#)]
32. Park, K.; Stokoe II, K.H.; Olson, R.E.; Seo, W. Settlements of footings in sand using dynamic soil properties. In *Soil-Foundation-Structure Interaction, Selected Papers Form International Workshop on Soil-Foundation Structure Interaction, Auckland*; Taylor & Francis Group: London, UK, 2010.
33. Sert, S.; Kiliç, A.N. Numerical Investigation of Different Superstructure Loading Type Effects in Mat Foundations. *Int. J. Civ. Eng.* **2016**, *14*, 171–180. [[CrossRef](#)]
34. Gusmão, A.D. Study of Soil-Structure Interaction and its Influence on Building Settlements. Master's Thesis, COPPE, UFRJ, Rio de Janeiro, Brazil, 1990.
35. Savaris, G.; Hallak, P.H.; Maia, P.C.A. Understanding the Mechanism of Static Soil-Structure Interaction—A Case Study. *Soils Rocks* **2011**, *34*, 195–206. [[CrossRef](#)]
36. Gonçalves, J.C.; Santa Maria, P.E.L.; Danziger, F.A.B.; Carvalho, E.M.L. The Influence of the Foundation Settlements on the column Loads of a Building. *Soils Rocks* **2007**, *30*, 149–159. [[CrossRef](#)]
37. Buttling, S.; Rui, Z. Settlement of high-rise building under construction—Measurement and modelling. In Proceedings of the 19th International Conference on Soil Mechanics and Geotechnical Engineering, Seoul, Republic of Korea, 17–21 September 2017; pp. 1815–1818.
38. Angelo Mussi, F.T.; Petrella, F.; Pisano, F. Settlement prediction and monitoring a piled raft foundation on coarse-grained soil: The case of the Allianz Tower in Milan. In Proceedings of the 19th International Conference on Soil Mechanics and Geotechnical Engineering, Seoul, Republic of Korea, 17–21 September 2017; pp. 2873–2876.
39. Shoaie, M.D.; Huat, B.B.K.; Jaafar, M.S.; Alkarni, A. Soil-Framed Structure interaction analysis—A new interface element. *Latin Am. J. Solids Struct.* **2015**, *12*, 226–249. [[CrossRef](#)]
40. Briançon, L.; Dias, D.; Simon, C. Monitoring and numerical investigation of a rigid inclusion-reinforced industrial building. *Can. Geotech. J.* **2015**, *52*, 1592–1604. [[CrossRef](#)]
41. Shoaie, M.D.; Huat, B.B.H.; Alkarni, A. Review of static soil-framed structure interaction. *Interact. Multiscale Mech.* **2013**, *6*, 51–81.
42. *Finite Element Program for Modeling, Analysis and Design of Any Type of Structure*, SAP2000 v. 22.1; CSI: Lisboa, Portugal, 2020.
43. Teixeira, A.H.; Godoy, M.S. Análise, projeto e execução de fundações rasas. In *Fundações: Teoria e Prática*; Hachich, W., Ed.; PINI: São Paulo, Brazil, 1998.
44. *Professional Software from GEOTEC Software*, ELPLA 10.1; GEOTEC: Calgary, AB, Canada, 2022.
45. Patricio, J.D. Performance Evaluation of Radiers in the Recife Metropolitan Region. Ph.D. Thesis, Federal University of Pernambuco, Recife, Brazil, 2019; 209p. (In Portuguese).
46. *CEB-FIP 90; CEB-FIP Model Code for Concrete Structures*. Comité Euro-International Du Béton (CEB): Lausanne, Switzerland, 1990.

**Disclaimer/Publisher's Note:** The statements, opinions and data contained in all publications are solely those of the individual author(s) and contributor(s) and not of MDPI and/or the editor(s). MDPI and/or the editor(s) disclaim responsibility for any injury to people or property resulting from any ideas, methods, instructions or products referred to in the content.